Computer Networks and Communications
https://ojs.wiserpub.com/index.php/CNC/

Research Article

Energy-Efficient MIMO Diversity: Operating Regimes, Hardware Constraints and Geometry-Aware Propagation Effects

Nikolaos Mouziouras*, Constantinos T. Angelis

Department of Informatics and Telecommunications, University of Ioannina, Arta, 47100, Greece
E-mail: n.mouziouras@uoi.gr

Received: 4 June 2026; **Revised:** 13 July 2026; **Accepted:** 20 July 2026; **Published:** 18 September 2026

Abstract: Multiple-Input Multiple-Output (MIMO) diversity techniques are widely employed to improve communication reliability in wireless systems; however, their energy-efficiency benefits under realistic propagation and hardware constraints remain insufficiently understood. This paper investigates the energy–reliability trade-off in MIMO diversity systems by jointly considering distance-dependent path loss, spatial correlation, retransmission effects and implementation-related energy costs. Representative diversity configurations, including Single-Input Single-Output (SISO) (1×1), Single-Input Multiple-Output (SIMO) (1×2) and Alamouti-based schemes (2×1 and 2×2), are evaluated across varying transmission distances and operating Signal-to-Noise Ratio (SNR) conditions. The results reveal a strongly operating-regime-dependent and non-monotonic relationship between diversity order and energy efficiency. Higher-order diversity is beneficial mainly in intermediate regimes, where reducing retransmissions can outweigh the additional implementation energy cost. Under favorable propagation conditions, however, implementation overhead dominates and lower-complexity configurations are more energy efficient. Conversely, under severely degraded conditions, all schemes enter a reliability-limited regime in which additional diversity provides diminishing energy returns. Furthermore, comparison with conventional Independent and Identically Distributed (i.i.d.) Rayleigh fading shows that simplified channel models systematically overestimate the achievable energy benefits of diversity techniques. The analysis identifies distinct operating regimes governing diversity-related energy efficiency and highlights the combined influence of propagation characteristics, reliability requirements, and hardware constraints. Overall, the results demonstrate that diversity is advantageous only under specific operating conditions, emphasizing the importance of operating-point-aware antenna configuration in practical wireless systems.

Keywords: Multiple-Input Multiple-Output (MIMO) systems, diversity techniques, energy efficiency, energy–reliability trade-off, geometry-aware channel modeling

Abbreviation

AWGN	Additive White Gaussian Noise
BER	Bit Error Rate
BPSK	Binary Phase-Shift Keying
CSI	Channel State Information
i.i.d.	Independent and Identically Distributed

Copyright ©2026 Nikolaos Mouziouras, et al.
DOI: https://doi.org/10.37256/cnc.42202610258
This is an open-access article distributed under a CC BY license
(Creative Commons Attribution 4.0 International License)
https://creativecommons.org/licenses/by/4.0/

IoT	Internet of Things
LOS	Line-of-Sight
LTE-A	Long-Term Evolution Advanced
MIMO	Multiple-Input Multiple-Output
MRC	Maximum Ratio Combining
NLOS	Non-Line-of-Sight
PER	Packet Error Rate
RF	Radio Frequency
SIMO	Single-Input Multiple-Output
SISO	Single-Input Single-Output
SNR	Signal-to-Noise Ratio
STBC	Space–Time Block Coding
UMi	Urban Microcell

1. Introduction

Multiple-Input Multiple-Output (MIMO) techniques are widely used in modern wireless communication systems to improve link reliability through spatial diversity [1]-[4]. By exploiting multiple antennas at the transmitter and/or receiver, diversity schemes such as Maximum Ratio Combining (MRC) and Space–Time Block Coding (STBC) effectively mitigate channel fading and improve communication robustness.

Despite these reliability benefits, the achievable energy-efficiency gains of MIMO diversity under realistic propagation and hardware constraints remain highly dependent on the operating conditions, particularly in energy-constrained systems such as wireless sensor networks and Internet of Things (IoT) devices [5], [6]. In such scenarios, communication typically dominates total energy consumption, while multiple antennas introduce additional hardware and signal-processing costs associated with Radio-Frequency (RF) chains and baseband processing. Consequently, increasing the diversity order does not necessarily improve energy efficiency, giving rise to a fundamental trade-off between reliability and energy consumption.

Most existing studies analyze MIMO performance under simplified channel assumptions, primarily based on Independent and Identically Distributed (i.i.d.) Rayleigh fading. However, such models neglect important characteristics of practical wireless environments, including distance-dependent path loss and spatial correlation between antenna elements. These effects can substantially influence both reliability and energy consumption, potentially leading to overly optimistic predictions regarding the energy benefits of diversity techniques [7]-[9].

Motivated by these limitations, this paper investigates the energy–reliability trade-off in MIMO diversity systems under realistic propagation and hardware constraints. A geometry-aware channel model is adopted to capture large-scale propagation effects and spatial correlation, enabling a more realistic representation of practical deployment scenarios. In addition, a unified evaluation framework is developed by combining packet-level performance analysis with a parameterized energy consumption model that explicitly accounts for retransmissions, circuit energy, and processing overhead. This framework enables the analysis of the operating regimes under which diversity improves or degrades energy efficiency.

The novelty of the present work lies in the joint consideration of propagation-aware MIMO diversity performance, packet-level reliability, retransmission-aware energy consumption and normalized hardware-overhead sensitivity. Unlike previous MIMO energy-efficiency analyses that typically focus on transmit power, spectral efficiency, idealized fading assumptions or hardware-specific energy models, the proposed framework links physical-channel realism with packet-level energy per successful transmission. This enables the identification of operating regimes in which either higher-order diversity or lower-complexity antenna configurations become preferable, depending on the propagation conditions, packet error behavior and relative circuit and processing overhead.

The main contributions of this work are threefold:

• A unified packet-level and propagation-aware framework for evaluating the energy–reliability trade-off of diversity-based MIMO configurations. In contrast to conventional analyses based mainly on abstract Signal-to-Noise Ratio (SNR) models or idealized fading assumptions, the proposed framework incorporates distance-dependent path loss, spatial correlation and geometry-dependent propagation effects.

• A retransmission-aware energy-efficiency analysis that links packet error behavior with the expected energy required for successful packet delivery. This allows the energy benefit of MIMO diversity to be evaluated beyond transmit-power considerations, explicitly accounting for packet-level reliability and normalized circuit- and processing-related overhead.

• Identification of operating regimes and transition conditions that determine when higher-order diversity becomes energy-beneficial and when lower-complexity antenna configurations remain preferable. The analysis further shows that simplified i.i.d. Rayleigh assumptions may overestimate diversity-related energy gains under realistic propagation conditions.

The remainder of this paper is organized as follows. Section 2 reviews related work and positions the main contributions of this study. Section 3 presents the system model and methodology. Section 4 discusses the simulation results and analytical insights. Finally, Section 5 concludes the paper.

2. Related work

A substantial body of literature has addressed energy-efficient MIMO system design. Early studies demonstrated that multi-antenna and cooperative transmission can reduce retransmissions and improve energy efficiency [5]. Subsequent works developed link-level optimization frameworks, typically based on abstract SNR models and idealized channel assumptions [6], [10], while the impact of Channel State Information (CSI) has also been investigated in terms of estimation–energy trade-offs [11].

More recent research has extended the analysis toward adaptive MIMO operation, energy-aware transmission strategies and realistic power-consumption modeling. Representative examples include adaptive massive MIMO operation under practical resource constraints [12], risk-aware antenna selection under incomplete CSI [13], and realistic non-linear power-consumption models for energy-efficient MIMO operation [14]. Complementary studies have also investigated finite-blocklength energy-efficiency optimization for MIMO systems [15]. Although these studies significantly advance individual aspects of practical MIMO system design, they generally examine adaptation, reliability or energy consumption separately and do not provide a unified packet-level framework that jointly captures realistic propagation, retransmission behavior and normalized hardware-related energy overhead.

A major limitation of existing work lies in the adopted channel models. Most studies assume simplified statistical fading models, primarily based on Independent and Identically Distributed (i.i.d.) Rayleigh fading, which neglect geometry-dependent propagation effects. In practical wireless environments, spatial correlation, multipath structure, and array geometry significantly influence MIMO performance [7]-[9], [16], [17]. As a result, simplified channel assumptions may substantially overestimate the achievable diversity and energy-efficiency gains.

In addition, prior work often evaluates reliability under asymptotic assumptions, overlooking finite-blocklength effects that are critical for packet-level communication performance [18]. This limitation is particularly important in practical low-power systems, where retransmissions dominate energy consumption and directly couple reliability with energy efficiency.

The positioning of the proposed work with respect to the existing literature is summarized in Figure 1 and Table 1. Figure 1 groups representative studies according to the main research directions that they address, including energy-efficient MIMO design, adaptive and system-level energy-efficiency optimization, realistic and spatially correlated MIMO channel modeling, and finite-blocklength reliability. Table 1 complements this overview by highlighting the extent to which these research directions cover the principal components of the proposed framework.

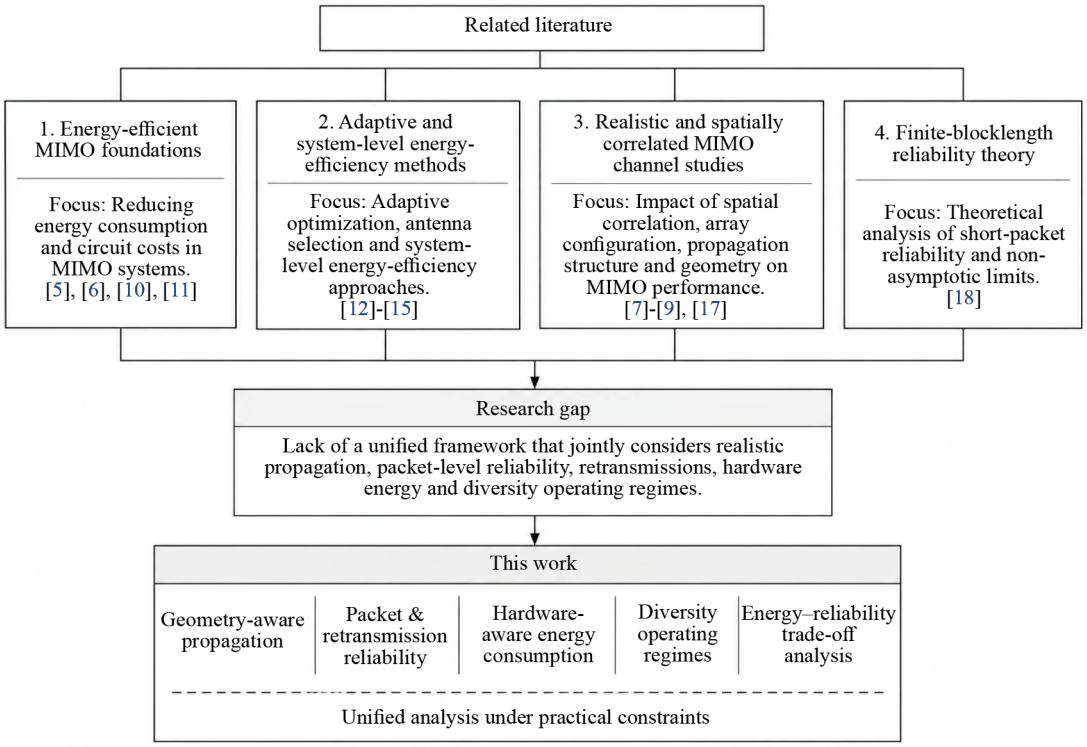


Figure 1. Literature positioning, identified research gap, and scope of the proposed framework

Table 1. Coverage of the main aspects addressed by the proposed framework

Ref(s).	Research group	Prop.	Pkt.	HW	Reg.
Cui et al. [5], Chen et al. [6], Isheden et al. [10], Rosas and Oberli [11]	Energy-efficient MIMO foundations	○	○	✓	○
Kim et al. [19], He et al. [20], Lee [21], Bao et al. [22]	Recent adaptive and system-level energy-efficiency methods	○	○	○	×
Forenza et al. [7], Tataria et al. [8], Ozdogan et al. [9], Chiani et al. [17]	Spatially correlated and realistic MIMO channel studies	✓	×	×	×
Polyanskiy et al. [18]	Finite-blocklength reliability theory	×	✓	×	×
This work	Unified MIMO diversity energy-efficiency framework	✓	✓	✓	✓

Legend: Prop. = Realistic Propagation; Pkt. = Packet/Retransmission Reliability; HW = Hardware-Aware Energy; Reg. = Diversity-Regime Analysis; ✓ = Main focus; ○ = Partially addressed; × = Not a primary focus

Overall, the proposed framework combines research directions that have largely been investigated separately in the existing literature. Previous MIMO energy-efficiency analyses have primarily focused on transmit-energy optimization, abstract link-level models or energy–reliability trade-offs under simplified channel assumptions [5], [6], [10]. Rather than introducing a new hardware power-consumption model, the framework jointly analyzes geometry-aware propagation, packet-level reliability, retransmission-aware energy consumption and normalized hardware-overhead sensitivity within a unified evaluation methodology. This enables the identification of operating regimes in which different MIMO diversity configurations become energy-optimal under realistic propagation conditions. This positioning distinguishes the proposed framework from previous MIMO energy-efficiency analyses and clarifies its practical design relevance.

3. System model and methodology

This section presents the system model and methodology used to analyze the energy–reliability trade-off in the considered MIMO diversity configurations. The communication link is represented using a flat-fading baseband model describing the interaction between transmitted signals, propagation effects, and receiver processing. To enable realistic performance evaluation, the proposed framework incorporates geometry-aware propagation modeling including distance-dependent path loss together with spatial correlation effects between antenna elements [7], [8], [17], while also considering packet-level performance metrics relevant to short-packet communication scenarios [18]. The overall methodology, illustrated in Figure 2, integrates channel modeling, packet-level reliability evaluation, and hardware-aware energy analysis within a unified simulation framework.

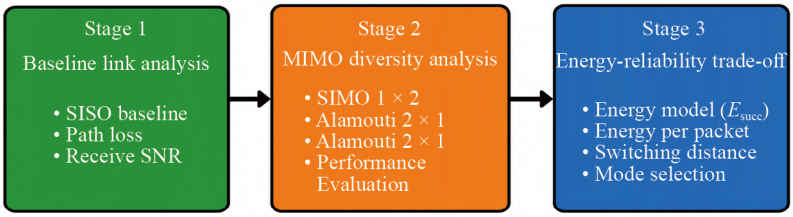


Figure 2. Proposed geometry-aware evaluation framework

The following subsections describe the signal model, performance metrics, and simulation methodology.

3.1 *Signal model*

A point-to-point uplink MIMO communication system is considered, where a transmitter equipped with N_t antennas communicates with a receiver employing N_r antennas. The analysis focuses on diversity-oriented configurations, including 1×1, 1×2, 2×1, and 2×2, allowing consistent comparison between single-antenna and diversity-based transmission schemes.

The discrete-time baseband received signal is expressed as

$$\boldsymbol{y} = \boldsymbol{H}\boldsymbol{x} + \boldsymbol{n}, \tag{1}$$

where $\boldsymbol{y} \in C^{N_r \times 1}$ denotes the received signal vector, $\boldsymbol{H} \in C^{N_r \times N_t}$ is the channel matrix, $\boldsymbol{x} \in C^{N_t \times 1}$ represents the transmitted signal vector and $\boldsymbol{n}$ is Additive White Gaussian Noise (AWGN).

The channel matrix $\boldsymbol{H}$ follows a geometry-aware formulation incorporating both large-scale propagation effects and small-scale fading [21]. Distance-dependent path loss is included to account for attenuation as a function of transmitter–receiver separation, while small-scale fading models the effects of multipath propagation. Unlike conventional i.i.d. channel assumptions, spatial correlation between antenna elements is explicitly incorporated, enabling more realistic characterization of effective diversity gains and propagation behavior.

When a single transmit antenna is employed (1×1 and 1×2 configurations), the system operates in Single-Input Single-Output (SISO) or Single-Input Multiple-Output (SIMO) mode, respectively, where receive diversity is exploited. For configurations with two transmit antennas (2×1 and 2×2), transmit diversity is enabled through the Alamouti space–time block coding scheme, which achieves full diversity gain with relatively low implementation complexity. To ensure a fair comparison across antenna configurations, the total transmit power is kept constant, such that the power allocated per transmit antenna is inversely proportional to N_t. This normalization avoids artificial performance gains caused by increased transmit power in multi-antenna schemes.

The average received Signal-to-Noise Ratio (SNR) is defined as

$$\gamma = \frac{P_t}{N_0}, \tag{2}$$

where P_t denotes the total transmit power and N_0 represents the noise power spectral density.

Due to fading and spatial correlation, the instantaneous SNR depends on the channel realization $\boldsymbol{H}$ as well as the applied diversity scheme. Receiver-side combining techniques, such as Maximum Ratio Combining (MRC) and transmit diversity schemes, such as Alamouti space–time block coding, exploit multiple faded signal components to improve the effective received signal power.

Under standard fading assumptions, the asymptotic Bit Error Rate (BER) behavior can be expressed as

$$\mathrm{BER} \propto \gamma^{-d}, \tag{3}$$

where d denotes the diversity order of the system. This relationship highlights that increasing diversity improves robustness against fading, leading to lower error probability and reduced retransmissions at the packet level.

The adopted system model provides a unified framework for evaluating the impact of antenna configuration and channel conditions on both reliability and energy efficiency, which are further analyzed in the following sections.

3.2 *Performance metrics and energy consumption model*

The system performance is evaluated using two metrics: Packet Error Rate (PER) and energy per successful packet transmission. Assuming independent bit errors, the packet error rate for a packet of length L can be approximated as

$$\mathrm{PER} \approx 1 - (1 - \mathrm{BER})^L, \tag{4}$$

indicating the strong sensitivity of packet-level reliability to the underlying bit error rate, particularly for short packets [4].

A normalized packet-level energy accounting model is adopted to evaluate the energy–reliability trade-off among the considered MIMO diversity configurations. The adopted model is now clearly presented as a normalized packet-level energy accounting framework, rather than a model intended to provide absolute hardware power-consumption measurements for a specific radio platform. Instead, it provides a relative energy comparison framework, in which all energy terms are expressed with respect to a reference packet transmit energy.

The reference energy E_{ref} is defined as the radiated transmit energy required to transmit one baseline SISO packet. In order to ensure a fair comparison among antenna configurations, the total packet transmit energy is kept constant across all modes and normalized as

$$E_{\mathrm{tx},\,m}^{\mathrm{pkt}} = E_{\mathrm{ref}}. \tag{5}$$

In the simulations, the packet length is $L_{\mathrm{pkt}} = 100$, and therefore the reference packet energy is set to $E_{\mathrm{ref}} = 100$ normalized energy units. Accordingly, all considered configurations use the same normalized radiated packet transmit energy in the baseline comparison. The additional energy costs associated with multiple RF chains, receiver-side combining and space–time processing are captured separately through the dimensionless coefficients α_m and β_m.

The normalized packet-energy cost of mode m, including transmit-energy, circuit-related and processing-related overheads, is modeled as

$$E_m^{\text{pkt}} = E_{\text{tx},\,m}^{\text{pkt}} + \alpha_m E_{\text{ref}} + \beta_m E_{\text{ref}}, \tag{6}$$

where α_m and β_m are dimensionless scaling coefficients representing the circuit-related and processing-related overheads of mode m, respectively. Since both overhead terms are scaled by E_{ref}, all terms in E_m^{pkt} have the same normalized energy dimension. The low, moderate and high overhead cases are therefore interpreted as parametric sensitivity regimes rather than empirical measurements from a specific hardware platform.

For the baseline retransmission-aware comparison, the hardware-overhead terms are not used to assign an empirical platform-specific cost. The nonzero overhead coefficients are introduced in the sensitivity analysis in order to examine how the preferred diversity mode changes as the relative circuit and processing cost increases.

Under independent retransmissions, the expected energy per successfully received packet for mode m is approximated as

$$E_m^{\text{succ}} = \frac{E_m^{\text{pkt}}}{1 - \text{PER}_m} = \frac{E_{\text{tx},\,m}^{\text{pkt}} + \alpha_m E_{\text{ref}} + \beta_m E_{\text{ref}}}{1 - \text{PER}_m}. \tag{7}$$

This expression accounts for the expected number of packet transmissions required to achieve one successful packet delivery, assuming independent retransmission attempts. As PER_m increases, the expected retransmission burden increases and therefore the energy per successful packet also increases [5], [6], [10].

The parameters α_m and β_m capture the hardware-dependent energy consumption associated with each antenna configuration. Specifically, α_m accounts for circuit-related energy, including RF chains and analog front-end components, while β_m represents the computational cost of baseband processing, which increases with receiver complexity and diversity scheme.

Three overhead regimes are considered: low, moderate and high. The low-overhead regime corresponds to energy-efficient hardware implementations, the moderate-overhead regime reflects practical operating conditions, while the high-overhead regime represents hardware-constrained scenarios dominated by circuit and processing energy consumption.

The adopted model is expressed in a normalized and parameterized form, enabling systematic sensitivity analysis without relying on hardware-specific implementations. This formulation separates retransmission-related energy from hardware-related energy, which is later used to interpret the regime-dependent behavior observed in Section 4.3.

3.3 *Simulation framework and evaluation methodology*

The analytical model described in the previous subsection defines the signal representation, antenna configurations and performance metrics. To evaluate the energy–reliability trade-off under realistic conditions, a simulation-based approach is adopted, following the processing chain illustrated in Figure 3.

The simulation framework includes channel realization generation, signal transmission, receiver processing, and packet-level error evaluation. Performance is assessed through Monte Carlo simulations, where multiple packet transmissions are generated for each operating point and the corresponding packet error rate is estimated. Independent channel realizations are generated during the Monte Carlo packet-level evaluation. A packet error is declared when at least one decoded symbol within the packet is erroneous.

Simulations were implemented using the Vienna Long-Term Evolution Advanced (LTE-A) Downlink System Level Simulator, release v2.0 (Q3-2018), as the baseline simulation framework [23]. The channel-generation routines were configured and adapted to explicitly control the propagation environment, Line-of-Sight (LOS)/Non-Line-of-Sight (NLOS) condition, distance-dependent path loss, small-scale fading, spatial correlation, antenna spacing, modulation and receiver processing. The main simulation parameters are summarized in Table 2, while the detailed channel-generation equations are provided in Section 4.3.

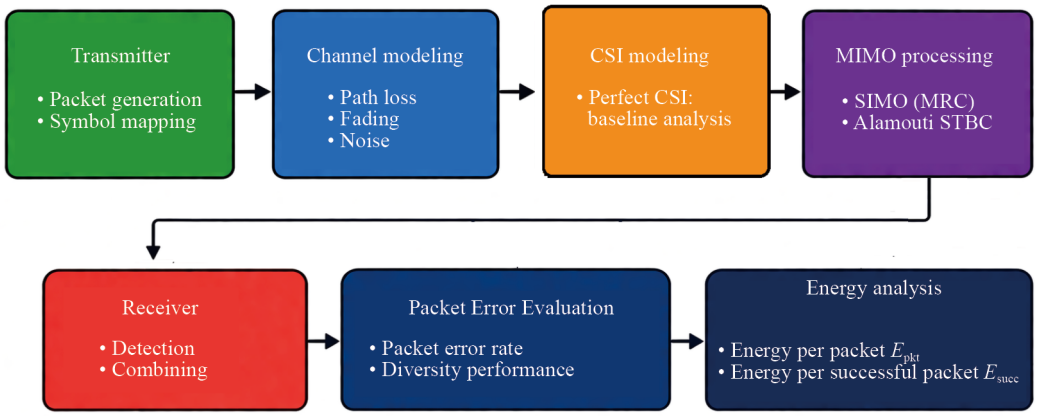


Figure 3. Simulation workflow for the considered MIMO diversity analysis

Table 2. Main simulation and channel-generation parameters

Parameter	Value/Assumption
Simulator framework	Vienna LTE-A Downlink System Level Simulator, release v2.0 (Q3-2018)
Carrier frequency	2.5 GHz
Propagation environments	Indoor LOS, Indoor NLOS, Urban Microcell (UMi) LOS and UMi NLOS
Path-loss model	Scenario-dependent log-distance formulation; see Appendix A
Small-scale fading	Rician fading for LOS links; Rayleigh fading for NLOS links
Rician factors	$K_{dB} = 6$ dB for Indoor LOS and $K_{dB} = 9$ dB for UMi LOS
Spatial correlation	Exponential transmit/receive correlation model; see Appendix A
Antenna configurations	SISO 1×1, SIMO 1×2, Alamouti 2×1, and Alamouti 2×2
Antenna spacing	0.5λ unless otherwise stated; varied from 0.1λ to 1.0λ in the antenna-spacing analysis
Distance range	5-50 m
Packet length	$L_{pkt} = 100$ Binary Phase-Shift Keying (BPSK) symbols, corresponding to 100 bits
Transmit-energy normalization	Equal total packet transmit energy across all antenna configurations; $E_{ref} = 100$ normalized energy units for $L_{pkt} = 100$
Modulation	BPSK
Channel coding	Not applied in the baseline Packet Error Rate (PER) evaluation
CSI assumption	Perfect CSI at the receiver unless otherwise stated
Receiver processing	Coherent SISO detection, receive-side combining for SIMO, and standard Alamouti decoding for 2×1 and 2×2 configurations
Monte Carlo evaluation	2,000-5,000 baseline; up to 20,000 for convergence validation

For each operating point, 2,000-5,000 packet transmissions are evaluated. This number was selected to provide consistent comparative trends across the considered operating regimes, rather than to provide asymptotically exact PER estimates. The packet length is fixed to 100 BPSK symbols, corresponding to 100 bits, representing a short-packet communication scenario relevant to IoT and low-latency wireless applications [22].

To further address the statistical reliability of the PER estimates, an additional convergence validation was performed for a representative simulation scenario. In particular, the same representative scenario was re-evaluated using 2,000, 10,000, and 20,000 packet transmissions. The results showed that increasing the number of transmitted packets reduces minor statistical fluctuations, especially in low-PER regions, while the overall PER trends and the relative performance

ranking of the considered MIMO configurations remain unchanged. The results obtained with 10,000 and 20,000 packet transmissions were very close, confirming that the reported PER estimates are statistically stable and that the main conclusions of the study are not affected by the selected number of packet transmissions.

To complement the Monte Carlo PER analysis under short-packet transmission, an additional finite-blocklength reliability validation was incorporated. While the main simulation framework evaluates the packet error rate directly through Monte Carlo packet transmissions, finite-blocklength information theory provides a complementary analytical framework to relate the packet size, coding rate, channel quality and decoding error probability. Therefore, for a representative validation scenario, the decoding error probability was also estimated using the normal approximation for finite-blocklength transmission.

For a given effective post-processing SNR γ, blocklength n and coding rate R, the decoding error probability is approximated as

$$\epsilon_{\mathrm{FBL}}(\gamma,\, n,\, R) \approx Q\left(\frac{C(\gamma)-R}{\sqrt{\frac{V(\gamma)}{n}}}\right). \tag{8}$$

In this expression, the channel capacity is given by

$$C(\gamma) = \log_2(1+\gamma), \tag{9}$$

while the corresponding channel dispersion is defined as

$$V(\gamma) = \left(1-\frac{1}{(1+\gamma)^2}\right)(\log_2(e))^2. \tag{10}$$

Here, γ denotes the effective post-processing SNR after the corresponding receive combining or space-time decoding operation.

In this validation, the number of information bits is set equal to the simulated packet size, i.e., $k = L_{\mathrm{pkt}} = 100$. For a given coding rate R, the corresponding blocklength is $n = k/R$. Representative coding rates $R = 0.5$ and $R = 0.75$ are considered in order to examine the sensitivity of the decoding error probability to finite-blocklength effects. This validation is intended to complement the Monte Carlo PER analysis by providing an information-theoretic reliability assessment under finite blocklength. It is not intended to replace the original Monte Carlo simulations or to represent the implementation of a specific practical channel code.

4. Simulation results

This section evaluates the considered antenna diversity configurations under geometry-aware propagation conditions. All configurations, namely SISO 1×1, SIMO 1×2, Alamouti 2×1, and Alamouti 2×2, are analyzed under equal transmit power constraints. The discussion focuses on distance-dependent behavior, operating conditions and hardware-aware energy effects. Unless otherwise stated, the reference receive SNR is set to 20 dB at 5 m.

4.1 *Energy–reliability trade-off versus distance*

The impact of transmission distance on packet-level reliability and energy efficiency is first examined under geometry-aware propagation conditions. Figure 4 shows that reliability generally improves with increasing diversity capability, although the exact ordering depends on the effective diversity gain achieved under the adopted geometry-aware propagation model and power normalization assumptions. In the considered Indoor LOS scenario, Alamouti 2×2 provides the strongest reliability performance, followed by SIMO 1×2, Alamouti 2×1, and SISO 1×1. This confirms the benefit of diversity-based transmission, while also showing that the relative performance of different MIMO configurations depends on the practical channel and combining conditions [1], [4].

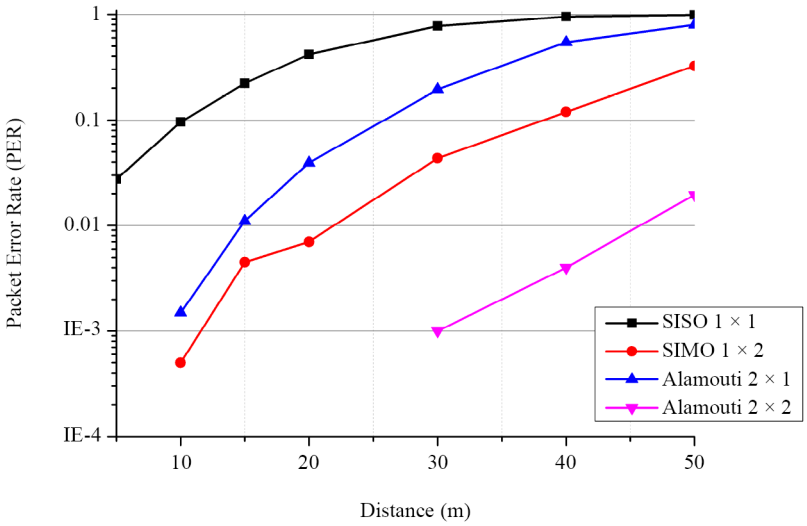


Figure 4. PER versus distance for the Indoor LOS scenario

The finite-blocklength validation further supports the reliability trends observed in the Monte Carlo PER simulations. For the higher representative coding rate $R = 0.75$, the decoding error probability increases as the transmission distance increases and the nominal large-scale SNR decreases. At 50 m, for example, the finite-blocklength decoding error probability increases to approximately 1.15×10^{-1} for SISO 1×1, while it remains significantly lower for the diversity-based configurations, reaching approximately 3.30×10^{-3} for SIMO 1×2, 1.60×10^{-2} for Alamouti 2×1 and 1.09×10^{-8} for Alamouti 2×2. These results confirm that the main reliability conclusions remain valid when coding rate, finite blocklength, channel dispersion and decoding error probability are explicitly taken into account.

Table 3. Energy per successful packet transmission for different antenna configurations

Distance (m)	SISO 1×1	SIMO 1×2	Alamouti 2×1	Alamouti 2×2	Best mode
5	102.82	100.00	100.00	100.00	1×2
10	110.68	100.05	100.15	100.00	2×2
15	128.36	100.45	101.11	100.00	2×2
20	171.23	100.70	104.11	100.00	2×2
30	441.50	104.54	124.14	100.10	2×2
40	2,197.80	113.63	218.81	100.40	2×2

However, improved reliability does not necessarily translate into improved energy efficiency. As shown in Table 3 and Figure 5, energy consumption remains nearly constant at short distances because packet error rates are negligible and retransmissions occur infrequently. Consequently, the total energy expenditure remains close to the nominal packet energy [5].

As transmission distance increases, retransmissions become the dominant contributor to total energy consumption. Consequently, low-diversity configurations such as SISO and Alamouti 2×1 exhibit rapidly increasing energy consumption due to sharply increasing PER. In contrast, higher-order diversity schemes substantially reduce retransmission-related energy, with Alamouti 2×2 maintaining the lowest or near-lowest energy consumption across most operating distances. Nevertheless, SIMO 1×2 remains highly competitive because of its lower hardware complexity. At large distances, the impact of severe path loss becomes increasingly dominant. Although all configurations experience reliability degradation, higher-order diversity schemes, particularly Alamouti 2×2, maintain substantially lower energy consumption by effectively limiting retransmissions.

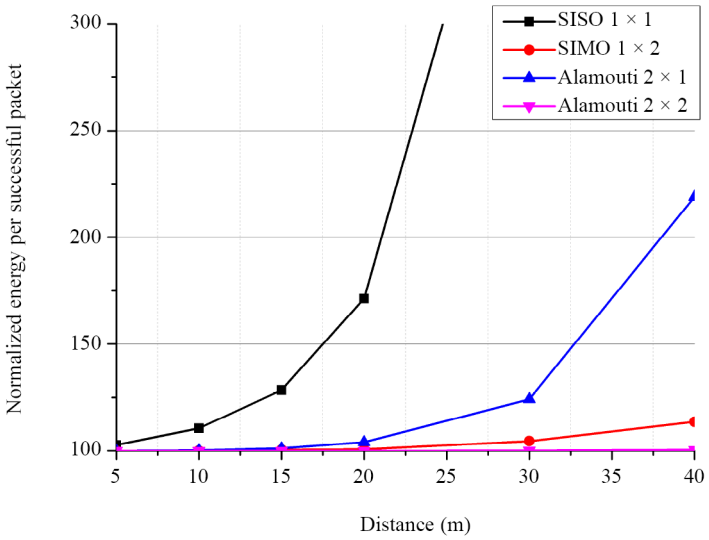


Figure 5. Energy per successful packet versus distance for the Indoor LOS scenario

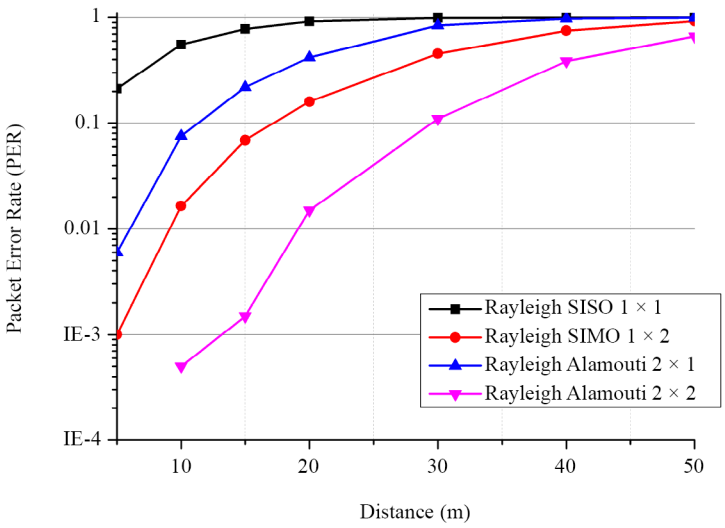


Figure 6. PER versus distance under the i.i.d. Rayleigh fading model

The importance of geometry-aware propagation modeling is further illustrated through comparison with an i.i.d. Rayleigh fading model in Figure 6. Simplified i.i.d. Rayleigh models neglect spatial correlation and geometry-dependent propagation effects, effectively assuming statistically independent diversity branches. As a result, such models tend to overestimate the achievable diversity and energy-efficiency gains [7], [8]. In contrast, the adopted geometry-aware framework captures propagation constraints that reduce the effective diversity gain under practical operating conditions, particularly at larger transmission distances where path loss and spatial correlation become increasingly significant.

Overall, the results show that the energy efficiency of diversity-based MIMO systems strongly depends on the operating regime. Diversity provides clear energy benefits primarily when retransmissions dominate system behavior, whereas under favorable channel conditions lower-complexity configurations remain more energy-efficient because of reduced hardware overhead.

4.2 *Impact of operating conditions*

To further examine the behavior of the considered diversity configurations, the analysis is extended to different operating conditions, including SNR, antenna spacing and propagation environment. These parameters directly affect channel reliability, spatial correlation and retransmission behavior, thereby influencing the resulting energy efficiency.

4.2.1 *Impact of SNR*

Figure 7 illustrates the general SNR-dependent energy trends of the two most energy-efficient diversity configurations across different operating regimes.

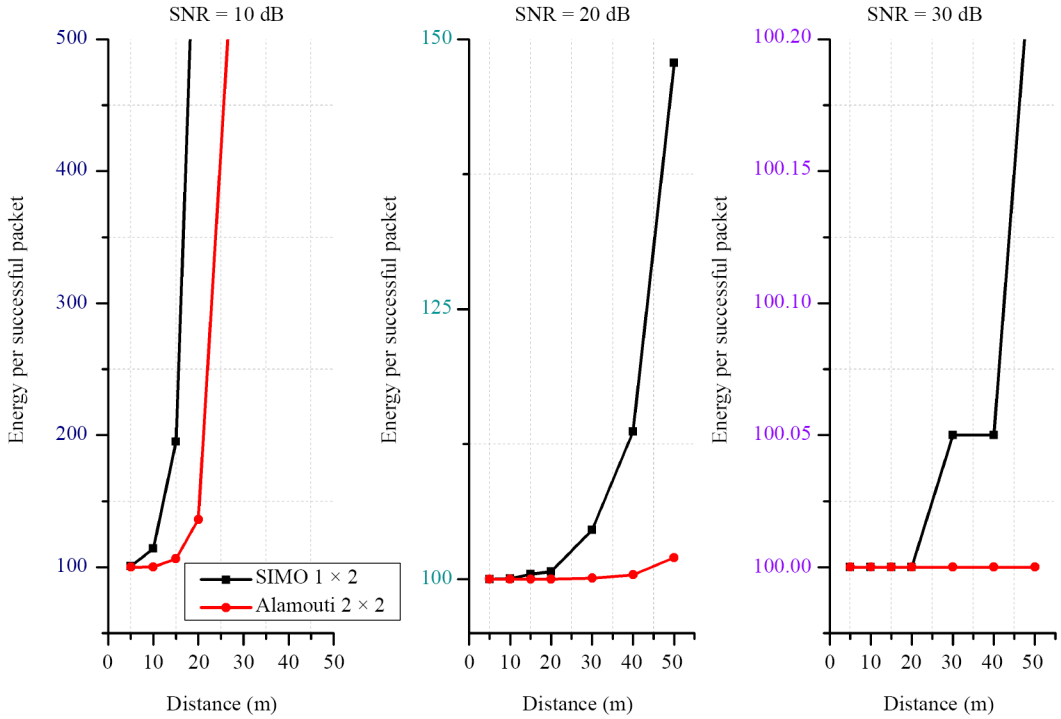


Figure 7. Impact of SNR on energy per successful packet versus distance

At low SNR, the system rapidly enters a reliability-limited regime in which retransmissions dominate energy consumption, leading to a sharp energy increase for lower-diversity configurations [4], [22]. In contrast, the Alamouti 2×2 scheme maintains substantially lower energy consumption because of its improved reliability. As SNR increases,

the energy–reliability trade-off becomes more pronounced, with higher-order diversity providing the largest practical energy benefit at moderate SNR values. Under these conditions, the Alamouti 2×2 configuration maintains nearly constant energy consumption across a wide distance range, while the energy consumption of SIMO 1×2 gradually increases as retransmissions become more frequent. At high SNR, all configurations achieve very low PER across the considered distance range. Consequently, retransmissions become negligible and energy consumption approaches the nominal transmit energy, reducing the relative energy advantage provided by higher-order diversity.

Overall, the results qualitatively confirm the distance-dependent behavior and show that SNR strongly influences the balance between retransmission-related energy and diversity gain. This behavior is also relevant to short-packet communication scenarios, where packet-level reliability is highly sensitive to symbol-error events. However, the present baseline evaluation does not apply an explicit finite-blocklength channel-coding model [18].

4.2.2 *Impact of antenna spacing*

The impact of antenna spacing is evaluated under Indoor LOS conditions at a fixed distance of 20 m and a reference SNR of 20 dB. Figure 8 shows that antenna spacing has a different impact depending on the diversity configuration. The Alamouti 2×2 scheme maintains very low PER across the considered spacing range, indicating reduced sensitivity to spatial correlation because of its higher diversity order. In contrast, the Alamouti 2×1 configuration exhibits slightly higher sensitivity to antenna spacing compared to Alamouti 2×2, with moderate performance variations across the considered spacing range. The SIMO 1×2 configuration remains comparatively stable across the considered operating conditions [7], [24].

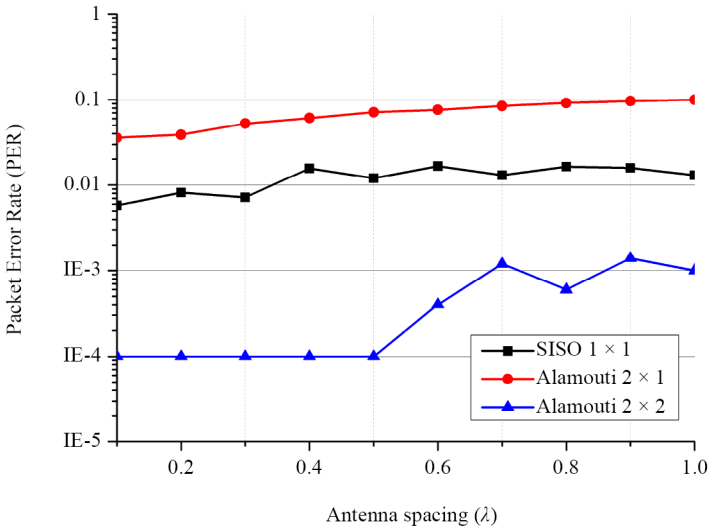


Figure 8. PER versus antenna spacing

The corresponding energy behavior shown in Figure 9 follows similar trends. The Alamouti 2×2 configuration maintains nearly constant energy consumption because of its consistently low PER, while SIMO 1×2 exhibits only minor energy variations. In contrast, the Alamouti 2×1 scheme exhibits slightly larger energy variations with antenna spacing because of its comparatively higher retransmission sensitivity.

Overall, antenna spacing has a secondary but non-negligible impact on system performance, primarily affecting configurations that are more sensitive to spatial correlation effects.

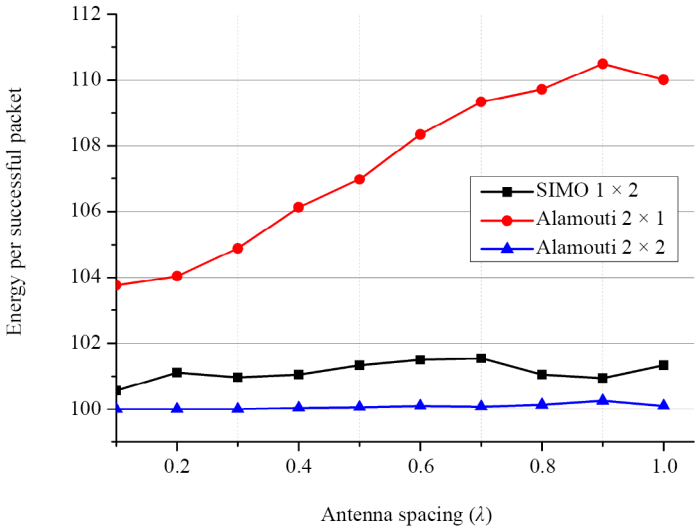


Figure 9. Energy per successful packet versus antenna spacing

4.2.3 *Impact of propagation environment*

The impact of the propagation environment on packet-level reliability is evaluated in Table 4.

Table 4. PER across propagation environments

Scenario	SISO 1 × 1	SIMO 1 × 2	Alamouti 2 × 1	Alamouti 2 × 2
Indoor LOS	0.0988	0.0002	0.0022	0.0000
Indoor NLOS	0.9998	0.9652	0.9999	0.9092
UMi LOS	0.0246	0.0000	0.0000	0.0000
UMi NLOS	1.0000	1.0000	1.0000	1.0000

Under LOS propagation, both Indoor and UMi scenarios achieve low PER values, with diversity schemes providing substantial reliability improvements. In particular, SIMO 1×2 and Alamouti 2×2 achieve extremely low packet error rates, while the UMi LOS scenario exhibits slightly better overall behavior because of more favorable propagation characteristics.

In contrast, reliability degrades significantly under NLOS conditions. For Indoor NLOS, the PER approaches unity for most configurations, although the Alamouti 2×2 scheme retains a limited diversity advantage. In the UMi NLOS scenario, all configurations exhibit PER ≈ 1, indicating outage-like operating conditions.

Overall, the results show that the achievable diversity gain is strongly environment-dependent. While LOS propagation enables substantial reliability improvements, severe NLOS conditions significantly limit the effectiveness of higher-order diversity schemes because of strong attenuation and increased channel variability [9], [21].

Overall, the results show that the energy–reliability behavior of diversity-based MIMO systems strongly depends on the operating conditions. Among the considered factors, SNR and propagation environment have the largest impact on reliability and retransmission-related energy consumption, while antenna spacing introduces secondary variations associated with spatial correlation effects. These observations further motivate the need for adaptive antenna configuration under realistic propagation conditions.

4.3 *Sensitivity analysis of the energy consumption model*

This subsection investigates the impact of hardware-related energy overhead on the energy–reliability trade-off and the resulting energy-optimal antenna configuration. Circuit and processing energy, which scale with the number of active antennas and receiver complexity, are modeled using the normalized parameters α_m and β_m introduced in Subsection 3.2.

The parameter values summarized in Table 5 reflect the relative increase in circuit and processing energy associated with increasing antenna configuration complexity. Configurations employing additional RF chains incur higher circuit-related energy consumption, while more sophisticated diversity schemes require increased baseband processing.

Table 5. α_m and β_m parameters

Configuration	α_m (Low)	β_m (Low)	α_m (Moderate)	β_m (Moderate)	α_m (High)	β_m (High)
SISO 1 × 1	0.10	0.00	0.50	0.00	1.00	0.00
SIMO 1 × 2	0.18	0.02	0.75	0.05	1.50	0.08
Alamouti 2 × 1	0.20	0.03	0.80	0.08	1.60	0.12
Alamouti 2 × 2	0.30	0.05	1.10	0.12	2.20	0.18

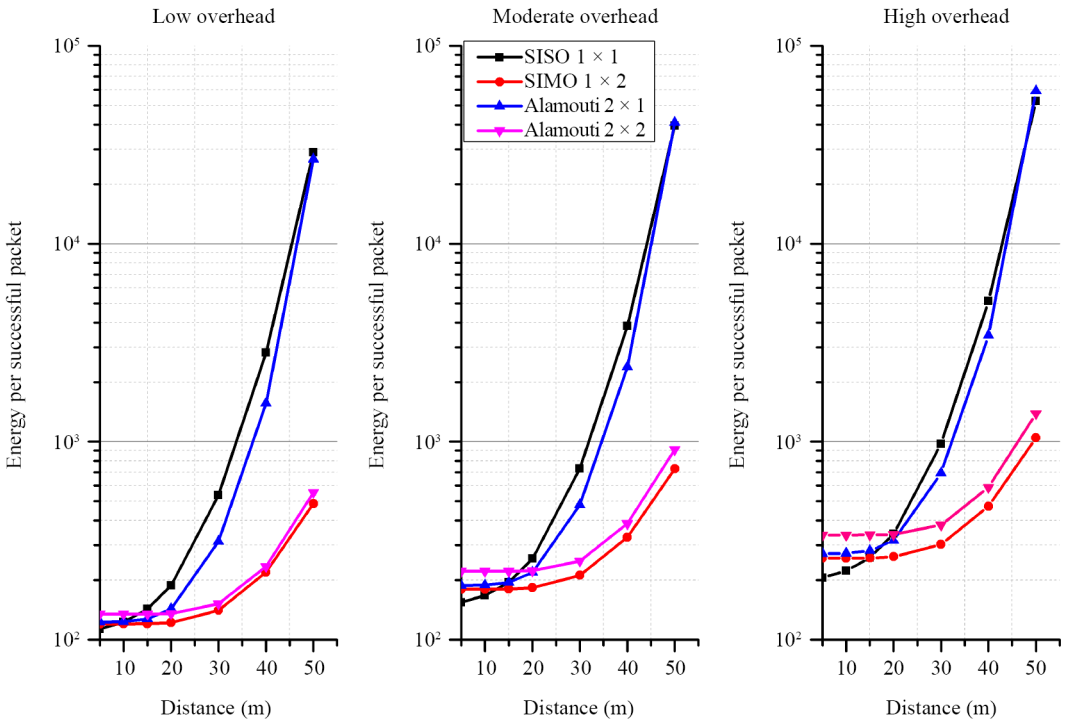


Figure 10. Energy per successful packet versus distance under different hardware-overhead regimes

The adopted parameter values are not tied to a specific hardware implementation but are selected to capture representative scaling trends, enabling systematic sensitivity analysis across a broad range of hardware conditions. Three overhead regimes are considered: low, moderate and high, corresponding to progressively increasing dominance of hardware-related energy consumption.

Figure 10 illustrates the energy per successful packet as a function of distance under these overhead regimes. Unlike the previous normalized-energy analysis, the present model explicitly incorporates hardware-dependent circuit and

processing overhead through the parameters α_m and β_m, enabling evaluation of the regime-dependent transition between retransmission-limited and hardware-limited operation.

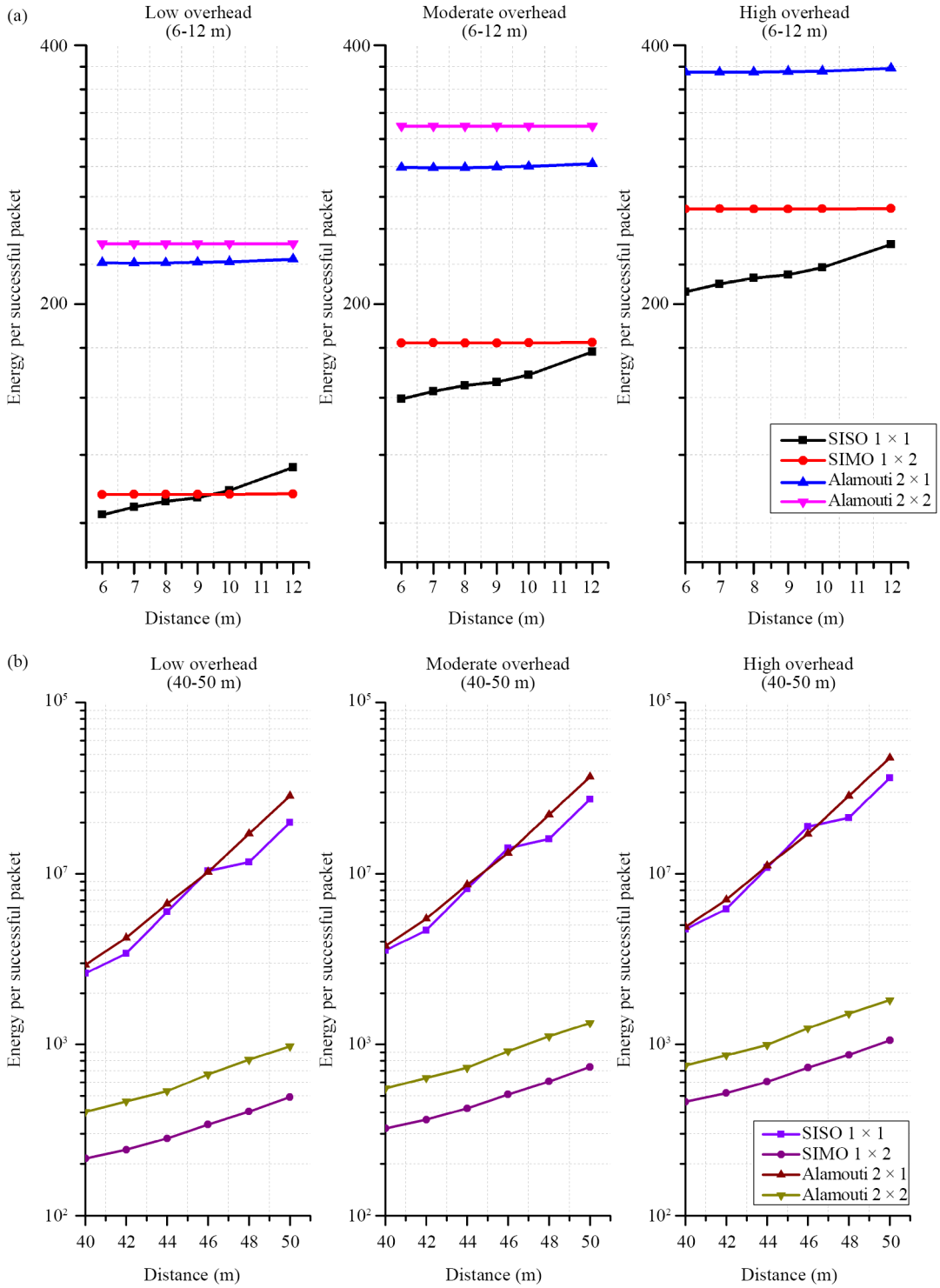


Figure 11. Energy per successful packet under different overhead conditions: (a) short-distance regime and (b) long-distance regime

Increasing hardware overhead raises the total energy consumption and significantly alters the relative ranking of antenna configurations. Under low-overhead conditions, higher-order diversity schemes remain competitive because reduced retransmissions compensate for the additional hardware cost. As hardware overhead increases, however, the energy cost associated with additional RF chains and processing complexity becomes progressively dominant, limiting the achievable benefit of higher-order diversity.

In moderate- and high-overhead regimes, SIMO 1×2 emerges as a competitive and in some cases energy-optimal, configuration across a broad range of operating distances by effectively balancing reliability improvements against hardware complexity.

Figure 11 further illustrates this behavior for two representative distance regimes. At short distances (6-12 m), packet error rates remain negligible and energy consumption is primarily determined by hardware-related overhead, favoring low-complexity configurations. At larger distances (40-50 m), retransmissions dominate total energy consumption. However, the additional diversity gain provided by the Alamouti 2×2 configuration becomes less effective in compensating for its increased hardware overhead, resulting in a reduced energy-efficiency advantage relative to SIMO 1×2.

Overall, the results reveal three distinct operating regimes. At short distances, energy consumption is dominated by circuit and processing overhead, making the system primarily hardware-limited. At intermediate distances, retransmissions become the dominant energy component, increasing the relative benefit of diversity. At large distances, severe PER degradation limits the achievable energy-efficiency gains for all configurations.

The transition between these regimes, as well as the energy-optimal antenna configuration, is strongly influenced by hardware-related energy overhead. As overhead increases, the optimal operating point progressively shifts toward lower-complexity diversity schemes.

These observations demonstrate that the relationship between diversity order and energy efficiency is inherently non-monotonic and jointly determined by propagation conditions and hardware constraints [5], [11].

4.4 *Design guidelines and analytical insights*

Based on the results presented in the previous sections, practical guidelines for energy-aware antenna configuration can be derived under geometry-aware propagation conditions.

The analysis reveals three distinct operating regimes. In the short-range regime (approximately 5-10 m), all configurations achieve very low PER and retransmissions remain negligible. Consequently, energy consumption is dominated primarily by hardware-related overhead, favoring lower-complexity configurations such as SIMO 1×2.

In the intermediate regime (approximately 10-40 m), retransmissions become increasingly important and the system behavior becomes reliability-driven. Under these conditions, higher-order diversity schemes provide significant energy-efficiency benefits because improved reliability compensates for the additional hardware overhead. However, the energy-optimal configuration remains dependent on the assumed hardware-overhead conditions.

In the edge-of-coverage regime (approximately 40-50 m), severe SNR degradation limits the achievable diversity gain and reduces the relative performance differences between antenna configurations. As a result, lower-complexity schemes become increasingly competitive under high-overhead conditions.

These observations indicate that antenna configuration should be selected adaptively according to the operating regime and hardware constraints.

The observed operating regimes can be interpreted analytically through the relationship between diversity, reliability, and energy consumption. For diversity-based systems, the asymptotic BER behavior can be expressed as

$$\mathrm{BER} \propto \mathrm{SNR}^{-d}, \tag{11}$$

where d denotes the diversity order [4].

At the packet level,

$$\mathrm{PER} = 1 - (1 - \mathrm{BER})^{L}, \tag{12}$$

indicating that improvements in BER directly reduce packet retransmissions.

Using the normalized energy model introduced in Subsection 3.2, the energy per successfully delivered packet for mode m is given by

$$E_m^{\mathrm{succ}} = \frac{E_m^{\mathrm{pkt}}}{1 - \mathrm{PER}_m}, \tag{13}$$

which highlights the strong dependence of energy consumption on packet reliability.

The observed trade-off arises from the balance between retransmission-related energy and hardware-related energy. Increasing diversity reduces PER and retransmissions, but also increases circuit and processing energy because of additional RF chains and signal-processing complexity.

A useful approximation for identifying regime transitions can be obtained by comparing these two energy components. The expected retransmission-related energy may be approximated as

$$E_{\mathrm{retx}} = E_{\mathrm{tx}} \frac{\mathrm{PER}}{1 - \mathrm{PER}}, \tag{14}$$

while the hardware-related energy is given by

$$E_{\mathrm{hw}} = E_{\mathrm{circuit}} + E_{\mathrm{proc}}. \tag{15}$$

The transition between hardware-limited and reliability-driven operation can therefore be approximated by the condition

$$E_{\mathrm{retx}} \approx E_{\mathrm{hw}}. \tag{16}$$

This condition provides a practical criterion for identifying when increasing diversity becomes beneficial from an energy-efficiency perspective. When retransmission-related energy dominates, higher-order diversity can reduce total energy consumption despite the additional hardware cost. Conversely, when hardware-related energy dominates, lower-complexity configurations become more energy-efficient.

Hardware overhead further shifts this balance. As circuit and processing energy increase, the relative benefit of higher-order diversity decreases, and configurations such as SIMO 1×2 become increasingly competitive despite their lower diversity order.

Overall, antenna mode selection should be treated as an adaptive process depending jointly on transmission distance, SNR, propagation conditions, and hardware constraints. The geometry-aware analysis reveals explicit operating regions and transition conditions, providing practical design guidelines for energy-efficient MIMO systems.

4.5 *Limitations of i.i.d. Rayleigh modeling in energy-efficient MIMO systems*

This subsection compares geometry-aware propagation with a conventional i.i.d. Rayleigh fading model, focusing on their impact on the energy–reliability trade-off. The analysis highlights how channel modeling assumptions directly influence the predicted energy efficiency of diversity-based transmission schemes.

To explicitly capture the energy cost associated with retransmissions, the same normalized energy-per-successful-packet metric defined in Eq. (13) is used.

$$E_{\text{succ}} = \frac{E_{\text{pkt}}}{1 - \text{PER}}, \tag{17}$$

which highlights the strong sensitivity of energy consumption to packet-level reliability.

As shown in Figure 12, the two channel models exhibit fundamentally different energy scaling behavior. Under geometry-aware propagation conditions, energy consumption increases rapidly with transmission distance for low-diversity configurations, with the SISO case exhibiting a sharp escalation beyond approximately 20-30 m because of increased retransmissions.

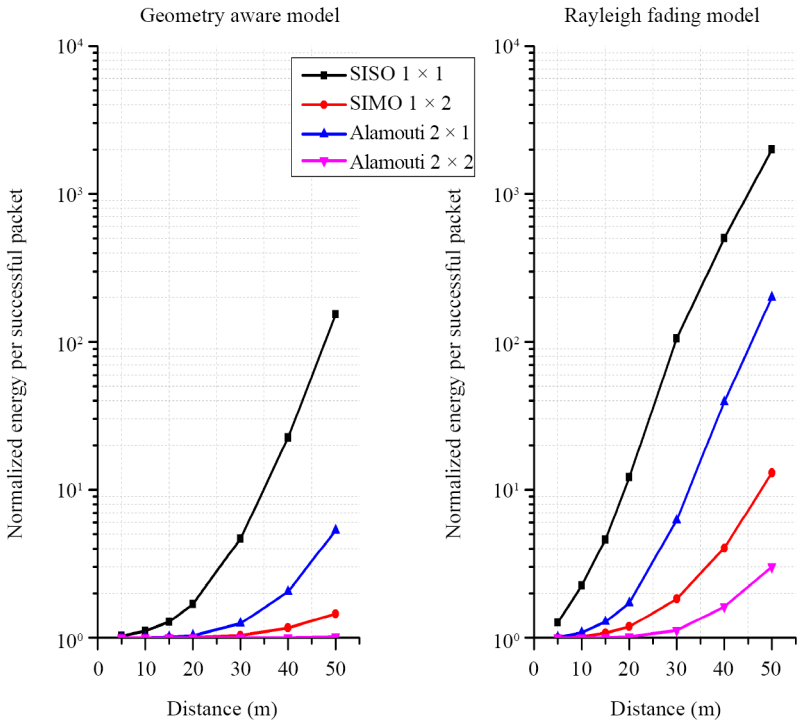


Figure 12. Comparison between geometry-aware and i.i.d. Rayleigh channel behavior in terms of energy per successful packet transmission

In contrast, higher-order diversity schemes, particularly the Alamouti 2×2 configuration, maintain comparatively lower energy consumption by effectively reducing packet errors and retransmission-related energy expenditure.

Under i.i.d. Rayleigh fading, however, all configurations appear substantially more energy-efficient and the increase in energy consumption with distance is considerably attenuated. Consequently, the diversity-induced energy gains appear significantly amplified and the achievable diversity benefit is systematically overestimated.

To quantify this effect, the normalized energy gain of the Alamouti 2×2 configuration relative to SISO is defined as

$$G(d) = \frac{E_{\text{succ}}^{\text{SISO}}(d)}{E_{\text{succ}}^{2\times 2}(d)}. \tag{18}$$

As shown in Figure 13, both channel models predict increasing diversity gain with transmission distance. However, the Rayleigh model exhibits significantly steeper gain growth, overestimating the achievable energy benefit at moderate and large distances.

In contrast, the geometry-aware model exhibits a more gradual increase together with a tendency toward saturation as the system approaches a reliability-limited operating regime.

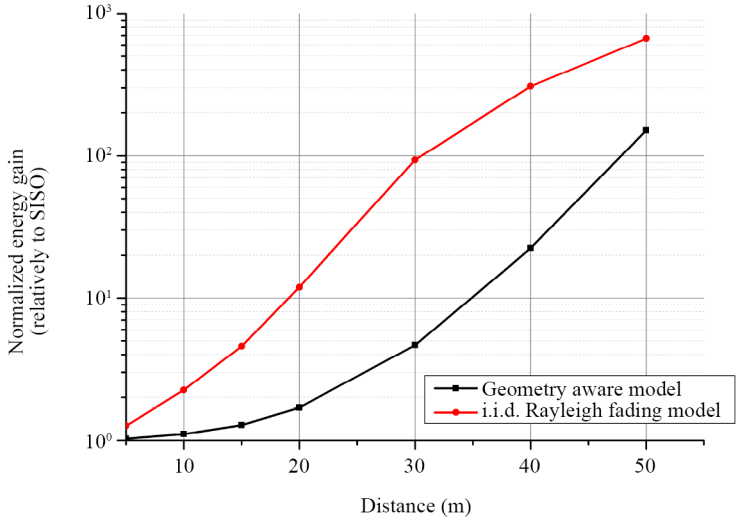


Figure 13. Comparison between geometry-aware and i.i.d. Rayleigh channel behavior in terms of normalized energy gain

This divergence originates from the underlying propagation assumptions. The i.i.d. Rayleigh model neglects spatial correlation and geometry-dependent channel structure, effectively assuming independent diversity branches. Such assumptions are known to overestimate diversity gains under realistic propagation conditions [7], [9].

By contrast, the geometry-aware model captures propagation constraints that limit the effective diversity gain, particularly at larger transmission distances where spatial correlation and path-loss effects become increasingly dominant.

Overall, the results demonstrate that although diversity improves reliability, its impact on energy efficiency is substantially constrained under realistic propagation conditions. Simplified channel models therefore lead to systematically optimistic predictions of diversity-related energy gains, particularly in operating regimes where retransmissions dominate system performance.

Most importantly, the results show that channel modeling assumptions directly influence system-level design decisions. Antenna configurations selected under i.i.d. Rayleigh assumptions may lead to overly optimistic expectations regarding achievable energy savings.

Under realistic geometry-aware propagation conditions, the effective diversity gain is constrained by path loss, spatial correlation and geometry-dependent channel structure. As a result, the energy-optimal antenna configuration is not determined solely by the nominal diversity order, but by the balance between reliability improvement, retransmission reduction and normalized hardware-related overhead. This can shift the preferred configuration toward lower-complexity schemes when the additional reliability benefit of higher-order diversity no longer compensates for the increased circuit and processing cost, especially in regimes where the energy–reliability trade-off is most pronounced.

4.6 *Key observations*

The presented results demonstrate that the energy efficiency of diversity-based MIMO systems strongly depends on the operating regime. At short transmission distances, energy consumption is dominated primarily by hardware-related overhead, favoring lower-complexity configurations. As transmission distance increases and retransmissions become the dominant energy component, higher-order diversity schemes provide increasing energy benefits through improved reliability.

The analysis further shows that geometry-aware propagation effects significantly influence the achievable diversity gain. Compared to idealized i.i.d. Rayleigh assumptions, realistic propagation conditions reduce the effectiveness of diversity because of spatial correlation and distance-dependent attenuation, leading to more constrained energy-efficiency gains.

An important observation is that the energy-optimal antenna configuration varies with propagation conditions, SNR, and hardware overhead. In many practical operating regions, moderate-diversity schemes such as SIMO 1×2 provide a favorable balance between reliability improvement and hardware complexity, while higher-order diversity becomes increasingly beneficial mainly in reliability-driven regimes.

Overall, these observations highlight the importance of geometry-aware and hardware-aware evaluation for the design of practical energy-efficient wireless communication systems.

5. Conclusion

This paper investigated the energy–reliability trade-off in MIMO diversity systems under geometry-aware propagation conditions. By combining packet-level reliability analysis with a parameterized energy model, a unified framework was developed to assess the behavior of different antenna configurations under realistic operating conditions.

The results demonstrate that increasing diversity does not necessarily improve energy efficiency. Instead, the relationship between diversity order and energy consumption is non-monotonic and strongly dependent on the operating regime. Higher-order diversity becomes beneficial primarily in conditions where retransmissions dominate total energy consumption, since improved reliability directly reduces the energy cost per successful packet. In contrast, when channel conditions are favorable and packet errors remain infrequent, energy consumption is mainly determined by hardware-related overhead, favoring lower-complexity configurations. At larger transmission distances and under harsh propagation conditions, all configurations gradually approach a reliability-limited regime in which the additional complexity of higher-order diversity provides only limited energy-efficiency gains.

An important outcome of this work is the demonstrated impact of geometry-aware propagation modeling. Compared to conventional i.i.d. Rayleigh assumptions, realistic propagation conditions introduce spatial correlation and distance-dependent constraints that limit the achievable diversity gains. As a result, simplified channel models systematically overestimate the energy efficiency of higher-order diversity configurations, particularly outside ideal operating conditions.

The analysis further shows that the energy-optimal antenna configuration is determined by the balance between retransmission-related energy and hardware overhead. This balance naturally defines different operating regimes and provides a practical basis for antenna selection. In this context, moderate-diversity schemes such as SIMO 1×2 often provide a favorable trade-off across a broad range of operating conditions, while higher-order diversity becomes advantageous mainly when reliability degradation becomes the dominant factor.

Overall, the results suggest that energy-efficient MIMO operation requires adaptive configuration strategies jointly accounting for propagation conditions, transmission distance, SNR, and hardware constraints. The proposed framework provides a systematic approach for identifying the relevant operating regimes and supports the design of energy-aware antenna selection mechanisms in practical wireless systems.

Future work will focus on adaptive energy-aware transmission strategies based on operating-regime identification, including dynamic antenna selection, adaptive diversity switching, and modulation and coding adaptation under geometry-aware propagation conditions. In addition, the proposed framework can be extended toward implementation-aware hardware modeling incorporating RF-chain power scaling, baseband processing complexity, and practical hardware

impairments. Another important direction involves extending the analysis to larger-scale MIMO configurations and cooperative transmission scenarios under realistic propagation environments.

Appendix A. Channel-generation details

This appendix provides the detailed channel-generation formulation used in the simulation framework. The simulations were implemented within a MATLAB-based framework using the Vienna LTE-A Downlink System Level Simulator, release v2.0 (Q3-2018), as the baseline simulation environment. Dedicated geometry-aware channel-generation functions were developed and incorporated to explicitly control the considered Indoor LOS, Indoor NLOS, UMi LOS, and UMi NLOS propagation conditions, including distance-dependent attenuation, small-scale fading, antenna spacing and spatial correlation.

The geometry-aware MIMO channel matrix is generated as

$$\boldsymbol{H} = \sqrt{G}\boldsymbol{R}_{\mathrm{rx}}^{1/2}\boldsymbol{H}_{\mathrm{small}}\boldsymbol{R}_{\mathrm{tx}}^{1/2}, \tag{A1}$$

where G is the large-scale linear channel gain, $\boldsymbol{R}_{\mathrm{tx}}$ and $\boldsymbol{R}_{\mathrm{rx}}$ are the transmit- and receive-side spatial correlation matrices, respectively, and $\boldsymbol{H}_{\mathrm{small}}$ is the small-scale fading matrix.

The large-scale gain is computed as

$$G = 10^{-(PL(d,\ f_c)+X_\sigma)/10}, \tag{A2}$$

where $PL(d,\ f_c)$ is the distance- and frequency-dependent path loss and X_σ is the log-normal shadowing term in dB. In the reported simulations, shadowing is disabled, i.e., $X_\sigma = 0$, in order to isolate the effects of distance-dependent path loss, small-scale fading and spatial correlation. When shadowing is enabled, X_σ is modeled as a zero-mean Gaussian random variable in dB, with scenario-dependent standard deviation, as summarized in Table A1.

Table A1. Scenario-dependent shadowing standard deviations

Scenario	σ_{sh} (dB)
Indoor LOS	3
Indoor NLOS	4
UMi LOS	4
UMi NLOS	6

A scenario-dependent log-distance surrogate path-loss model is adopted

$$PL(d,\ f_c) = A_s + B_s \log_{10}(d) + 20\log_{10}(f_c), \tag{A3}$$

where d is the transmitter–receiver distance in meters, f_c is the carrier frequency in GHz, and A_s, B_s are scenario-dependent coefficients. The distance is lower-bounded by 1 m to avoid singular behavior at very short distances. The coefficients used in the simulations are summarized in Table A2.

Table A2. Scenario-dependent path-loss coefficients

Scenario	A_s	B_s
Indoor LOS	32	17
Indoor NLOS	38	22
UMi LOS	30	21
UMi NLOS	36	31

For LOS links, the small-scale fading matrix follows a Rician formulation,

$$\boldsymbol{H}_{\text{small}} = \sqrt{\frac{K}{K+1}}\boldsymbol{H}_{\text{LOS}} + \sqrt{\frac{1}{K+1}}\boldsymbol{H}_{\text{NLOS}}, \tag{A4}$$

where $K = 10^{K_{\text{dB}}/10}$ is the Rician factor in linear scale. The values $K_{\text{dB}} = 6$ dB and $K_{\text{dB}} = 9$ dB are used for Indoor LOS and UMi LOS conditions, respectively. The NLOS component $\boldsymbol{H}_{\text{NLOS}}$ has independent circularly symmetric complex Gaussian entries. For NLOS propagation scenarios, the small-scale fading matrix is directly modeled as a Rayleigh fading matrix with independent complex Gaussian entries.

The deterministic LOS component is constructed from transmit and receive array response vectors as

$$\boldsymbol{H}_{\text{LOS}} = \boldsymbol{a}_{\text{r}}(\theta_r)\boldsymbol{a}_{\text{t}}^{T}(\theta_t), \tag{A5}$$

where θ_t and θ_r denote the transmit and receive angles, respectively. Unless fixed angles are specified, these angles are randomly drawn in the interval $[-\pi/2,\ \pi/2]$. Uniform linear arrays are assumed at both the transmitter and receiver. The angles θ_t and θ_r are measured with respect to the array broadside direction, and the antenna elements are placed along a linear axis with inter-element spacing $\Delta_{\text{tx}}\lambda$ and $\Delta_{\text{rx}}\lambda$, respectively.

The transmit and receive array response vectors are given by

$$\boldsymbol{a}_{\text{t}}(\theta_t) = \left[1,\ e^{j2\pi\Delta_{\text{tx}}\sin(\theta_t)},\ \ldots,\ e^{j2\pi\Delta_{\text{tx}}(N_t-1)\sin(\theta_t)}\right]^{T}, \tag{A6}$$

and

$$\boldsymbol{a}_{\text{r}}(\theta_r) = \left[1,\ e^{j2\pi\Delta_{\text{rx}}\sin(\theta_r)},\ \ldots,\ e^{j2\pi\Delta_{\text{rx}}(N_r-1)\sin(\theta_r)}\right], \tag{A7}$$

where Δ_{tx} and Δ_{rx} denote the transmit and receive antenna spacing normalized by the wavelength. Unless otherwise stated, $\Delta_{\text{tx}} = \Delta_{\text{rx}} = 0.5$.

The transmit- and receive-side spatial correlation matrices are modeled using an exponential correlation structure. For each propagation scenario, the base correlation coefficient is computed as

$$\rho_s = \exp\left(-\beta_s\Delta_\lambda\right), \tag{A8}$$

where Δ_λ is the antenna spacing normalized by the wavelength and β_s is a scenario-dependent decay parameter. The corresponding spatial correlation matrix is constructed as

$$[\boldsymbol{R}]_{i,\,j} = \rho_s^{|i-j|}, \tag{A9}$$

where i and j denote antenna indices. This formulation is applied separately at the transmitter and receiver sides, resulting in $\boldsymbol{R}_{\text{tx}}$ and $\boldsymbol{R}_{\text{rx}}$, respectively. The decay parameters used in the simulations are summarized in Table A3.

Table A3. Scenario-dependent spatial-correlation decay parameters

Scenario	β_s
Indoor LOS	1.8
Indoor NLOS	1.2
UMi LOS	1.5
UMi NLOS	1.0

Finally, the channel matrix may optionally be normalized according to its Frobenius norm. However, in the reported simulations, channel normalization is disabled so that the combined effects of distance-dependent path loss, fading and spatial correlation are preserved in the received signal strength.

Author contributions

N. Mouziouras: conceptualization, methodology, software, simulation, formal analysis, visualization, writing—original draft preparation; C.T. Angelis: validation, review and editing.

Funding

This research received no external funding.

Data availability

The data supporting the findings of this study are available from the corresponding author upon reasonable request.

Conflict of interest

The authors declare that they have no known competing financial interests or personal relationships that could have appeared to influence the work reported in this paper.

References

[1] S. M. Alamouti, "A simple transmit diversity technique for wireless communications," *IEEE Journal on Selected Areas in Communications*, vol. 16, no. 8, pp. 1451-1458, 1998. Available: https://doi.org/10.1109/49.730453.

[2] D. Tse and P. Viswanath, *Fundamentals of Wireless Communication*. Cambridge, U.K.: Cambridge University Press, 2005.

[3] A. Goldsmith, *Wireless Communications*. Cambridge, U.K.: Cambridge University Press, 2005.

[4] M. K. Simon and M.-S. Alouini, *Digital Communication over Fading Channels*, 2nd ed., New York: John Wiley & Sons, 2005.

[5] S. Cui, A. J. Goldsmith, and A. Bahai, "Energy-efficiency of MIMO and cooperative MIMO techniques in sensor networks," *IEEE Journal on Selected Areas in Communications*, vol. 22, no. 6, pp. 1089-1098, 2004. Available: https://doi.org/10.1109/JSAC.2004.830916.

[6] Y. Chen, S. Zhang, S. Xu, and G. Y. Li, "Fundamental trade-offs on green wireless networks," *IEEE Communications Magazine*, vol. 49, no. 6, pp. 30-37, 2011. Available: https://doi.org/10.1109/MCOM.2011.5783982.

[7] A. Forenza, D. J. Love, and R. W. Heath, "Simplified spatial correlation models for clustered MIMO channels with different array configurations," *IEEE Transactions on Vehicular Technology*, vol. 56, no. 4, pp. 1924-1934, 2007. Available: https://doi.org/10.1109/TVT.2007.897212.

[8] H. Tataria, S. Sangodoyin, A. F. Molisch, P. J. Smith, M. Matthaiou, J. Zhang, et al., "Channel correlation diversity in MU-MIMO systems: Analysis and measurements," in Proc. 2019 IEEE 30th Annual International Symposium on Personal, Indoor and Mobile Radio Communications (PIMRC), 2019, pp. 1-7. Available: https://doi.org/10.1109/PIMRC.2019.8904875.

[9] Ö. Özdogan, E. Björnson, and E. G. Larsson, "Massive MIMO with spatially correlated Rician fading channels," *IEEE Transactions on Communications*, vol. 67, no. 5, pp. 3234-3250, 2019. Available: https://doi.org/10.1109/TCOMM.2019.2893221.

[10] C. Isheden, Z. Chong, E. Jorswieck, and G. Fettweis, "Framework for link-level energy efficiency optimization with informed transmitter," *IEEE Transactions on Wireless Communications*, vol. 11, no. 8, pp. 2946-2957, 2012. Available: https://doi.org/10.1109/TWC.2012.060412.111829.

[11] F. Rosas and C. Oberli, "Impact of the channel state information on the energy-efficiency of MIMO communications," *IEEE Transactions on Wireless Communications*, vol. 14, no. 8, pp. 4156-4169, 2015. Available: https://doi.org/10.1109/TWC.2015.2417530.

[12] S. Marwaha, E. A. Jorswieck, M. S. Jassim, T. Kürner, D. L. Pérez, X. Geng, et al., "Energy efficient operation of adaptive massive MIMO 5G HetNets," *IEEE Transactions on Wireless Communications*, vol. 23, no. 7, pp. 6889-6904, 2024. Available: https://doi.org/10.1109/TWC.2023.3336059.

[13] K. He, T. X. Vu, D. T. Hoang, D. N. Nguyen, S. Chatzinotas, and B. Ottersten, "Risk-aware antenna selection for multiuser massive MIMO under incomplete CSI," *IEEE Transactions on Wireless Communications*, vol. 23, no. 9, pp. 11001-11014, 2024. Available: https://doi.org/10.1109/TWC.2024.3377733.

[14] R. Beerten, V. Ranjbar, H. Sallouha, and S. Pollin, "Cell-free massive MIMO under a non-linear power amplifier consumption model," in Proc. 2025 IEEE 26th International Workshop on Signal Processing and Artificial Intelligence for Wireless Communications (SPAWC), 2025, pp. 1-5. Available: https://doi.org/10.1109/SPAWC66079.2025.11143439.

[15] M. Soleymani, I. Santamaria, E. A. Jorswieck, R. Schober, and L. Hanzo, "Optimization of the downlink spectral- and energy-efficiency of RIS-aided multi-user URLLC MIMO systems," *IEEE Transactions on Communications*, vol. 73, no. 5, pp. 3497-3513, 2025. Available: https://doi.org/10.1109/TCOMM.2024.3480988.

[16] 3GPP, "Study on channel model for frequencies from 0.5 to 100 GHz," 3rd Generation Partnership Project (3GPP), Tech. Report. 3GPP TR 38.901, v16.1.0, 2019.

[17] M. Chiani, M. Z. Win, and A. Zanella, "On the capacity of spatially correlated MIMO Rayleigh-fading channels," *IEEE Transactions on Information Theory*, vol. 49, no. 10, pp. 2363-2371, 2003. Available: https://doi.org/10.1109/TIT.2003.817437.

[18] Y. Polyanskiy, H. V. Poor, and S. Verdu, "Channel coding rate in the finite blocklength regime," *IEEE Transactions on Information Theory*, vol. 56, no. 5, pp. 2307-2359, 2010. Available: https://doi.org/10.1109/TIT.2010.2043769.

[19] E. Kim, B. C. Jung, C. Y. Park, and H. Lee, "Joint optimization of energy efficiency and user outage using multi-agent reinforcement learning in ultra-dense small cell networks," *Electronics*, vol. 11, no. 4, p. 599, 2022. Available: https://doi.org/10.3390/electronics11040599.

[20] Z. He, W. Xu, H. Shen, Y. Huang, and H. Xiao, "Energy efficient beamforming optimization for integrated sensing and communication," *IEEE Wireless Communications Letters*, vol. 11, no. 7, pp. 1374-1378, 2022. Available: https://doi.org/10.1109/LWC.2022.3169517.

[21] B. M. Lee, "Leveraging massive MIMO for enhanced energy efficiency in high-density IoT networks," *Mathematics*, vol. 12, no. 22, p. 3539, 2024. Available: https://doi.org/10.3390/math12223539.

[22] B. Q. Bao, K. X. Thuc, and P. T. Hiep, "Short-packet communication for MIMO NOMA relay networks: BLER and AoI analysis," *AEU-International Journal of Electronics and Communications*, vol. 174, p. 155035, 2024. Available: https://doi.org/10.1016/j.aeue.2023.155035.

[23] M. Rupp, S. Schwarz, and M. Taranetz, *The Vienna LTE-Advanced Simulators*. Singapore: Springer, 2016.

[24] H. Luo, J. Tang, Z. Ou, Y. Liu, and H. Yang, "Enhance the performance of expectation propagation detection in spatially correlated massive MIMO channels via DFT precoding," *Entropy*, vol. 27, no. 10, p. 1030, 2025. Available: https://doi.org/10.3390/e27101030.